MDPI

Article

Oxygen Uptake of Ti6Al4V during Direct Metal Deposition Process

Dominik Keller [1],*, Axel Monney [1], Florian Wirth [2] and Konrad Wegener [1]

1 Institut Für Werkzeugmaschinen und Fertigung, ETH Zürich, Leonhardstrasse 21, 8092 Zürich, Switzerland; amonney@student.ethz.ch (A.M.)
2 Exentis Group AG, Im Stetterfeld 2, 5608 Stetten, Switzerland; f.wirth@exentis-group.com
* Correspondence: keller@iwf.mavt.ethz.ch

Abstract: The efficient fabrication of titanium components using laser direct metal deposition (DMD) is gaining significant importance in the aerospace and medical sectors. The DMD process must be appropriately designed to address the issue of oxidation, as titanium exhibits a high affinity for oxygen. The carrier gas flow and shield gas flow, which have been considered secondary factors so far, are shown to exert a substantial influence on the gas dynamics of the DMD process. By varying these parameters, it is possible to identify the influence of the gas volume flows on the oxidation behavior exhibited during the DMD process. To quantify the oxygen uptake in titanium structures during buildup, hot carrier gas extraction is employed. Experiments are conducted using both a three-jet and a coaxial nozzle to assess the influence of nozzle geometry. Additionally, the experiments are conducted within a shielding gas chamber to demonstrate the benefits of such a chamber in mitigating oxidation. Finally, the study reveals that by appropriately combining the parameters of carrier gas volume flow, shield gas volume, and travel speed, it is possible to fabricate titanium components, which fulfill the requirements regarding oxygen content of aerospace and medical applications even without the utilization of a shielding gas chamber.

Keywords: oxidation; DMD; hot carrier gas extraction; oxygen uptake; titanium; titanium alloys

1. Introduction

In contemporary industrial manufacturing, additive manufacturing processes are gaining increasing importance, primarily due to their free-forming nature and high material efficiency. These processes can be categorized based on the feedstock (powder, wire, etc.) and energy source (laser, electric current) used to melt the substrate and feedstock material [1]. This study focuses on investigating the direct metal deposition (DMD) process, wherein powder is injected through a nozzle into a melt pool created by a laser on a substrate. Previous research has extensively studied Fe- and Ni-based alloys in the DMD process, examining the impact of key machine parameters, such as laser power, travel speed, and powder mass flow, on the width, height, and crack formation of buildups [2–6]. The concept of linear heat input has been found effective in establishing suitable process parameters for most Fe- and Ni-based alloys, ensuring a strong metallurgical bond between the substrate and buildup material, and achieving high material density with low porosity [6,7]. However, the study of additive manufacturing with titanium and its alloys remains relatively underexplored. Titanium is of particular interest to the aerospace and medical industries due to its corrosion resistance, biocompatibility, and excellent strength-to-density ratio [8–11]. Yet, titanium differs from Fe- and Ni-based alloys as it has a high affinity for oxygen, necessitating an investigation of oxidation during the DMD process [12]. Oxidation can deteriorate the mechanical properties of titanium components [13]. Gurappa's research elucidates that the development of a hard and brittle oxygen diffusion zone under the oxide layer significantly impairs the high-temperature performance of titanium

alloys, resulting in reduced tensile strength and diminished fatigue resistance [14]. Moreover, Casadebaigt et al. demonstrates the embrittlement caused by oxidation in titanium fabricated by laser and electron melting [15].

Guleryuz and Cimenoglu [16] have investigated the oxidation behavior of Ti6Al4V in a temperature range of 600–800 °C based on the weight gain over time intervals of 0.5–72 h. Oxidation kinetics can be described by the equation,

$$\frac{\Delta W}{A} = K \cdot t^{1/n},\tag{1}$$

where $\frac{\Delta W}{A}$ is the normalized weight gain, K is the rate constant, t is the oxidation time and n is the reaction index. It is shown that in the range of 600–700 degrees Celsius, the oxidation kinetics can be described by a parabolic function (n equals 2). As a result, the oxidation rate decreases over time. Above 700 degrees Celsius, the oxidation kinetics can be described by a linear law (n equals 1), so that the oxidation rate remains constant over time. Various studies explain this behavior of oxidation kinetics. According to Du et al. [17], thermal expansion coefficient mismatch between the outer layer (OL) and the substrate generates high stresses, limiting OL adherence. Yu et al. [18] observed increased oxidation rates at 700 °C after 20 h due to OL failure. In a study of commercially pure titanium oxidation from 500–700 °C, Coddet et al. [19] noted that OL adhesion strength remained high below 650 °C but decreased to nearly zero at 700 °C.

A problem in the studies [8–19] is that the oxidation time period is not applicable to the DMD process because the melt pool lifetime can be calculated by the equation,

$$t_{melt} = \frac{s}{v},\tag{2}$$

where s is the laser focus diameter and v is its travel speed. The melt pool lifetime (assuming the machine parameters used in this study are, travel speed: 720 mm/min, laser spot diameter: 3 mm) is 0.25 s and thus does not fall within the range of the studies [8–19]. To solve this problem, different titanium samples are set up at different gas flow settings and different travel speeds. As pointed out in the work of Keller et al. [20] the nozzle geometry, carrier gas, and shield gas volume flow have a significant effect on the spatially present oxygen concentration.

The aim of this work is to transfer the quasi-static simulation and oxygen measurements in the work of Keller et al. [20] to the resulting oxidation of the DMD structure of Ti6Al4V. Thus, the influence of the dynamics of the process on the oxidation of Ti6Al4V can be investigated. To meet industry standards, the maximum permissible oxygen concentration in titanium components is defined in DIN 17850 [21] for pure titanium and DIN 17851 [22] for titanium alloys such as Ti6Al4V (Titanium Grade 5, O_{max} = 2000 ppm for aerospace industry) and Grade 23 (Ti6Al4V extra low interstitials (ELI), O_{max} = 1300 ppm for medical industry). Finally, limit values for the carrier gas, shielding gas flow rates, and travel speed should be developed, which can be used to build titanium components that meet the requirements of the aerospace and medical industry.

This study aims to investigate and analyze the impact of shielding gas volume flow, carrier gas volume flow, the usage of a shielding gas chamber, and travel speed on the oxidation during the DMD process.

2. Materials and Methods

A Yb:YAG laser (TruDisk 3001) with a wavelength of 1030 nm and a maximum laser output power of 3 kW was used for the DMD experiments. The powder was delivered to the powder nozzle by the powder feeder via antistatic hoses. The powder was coaxially injected into the laser-generated melt pool on a Ti6Al4V substrate via an argon carrier gas stream. Two different nozzle geometries were used to evaluate the influence of the nozzle geometry: a coaxial nozzle and a three-jet nozzle. The Ti6Al4V powder particles were manufactured by electrode induction melting inert gas atomization from the company

Oerlikon Metco, 5610 Wohlen, Switzerland. The powder particle fraction is between 45–105 μm (D_{50} = 68 μm) and the particles were spherical as shown in Figure 1.
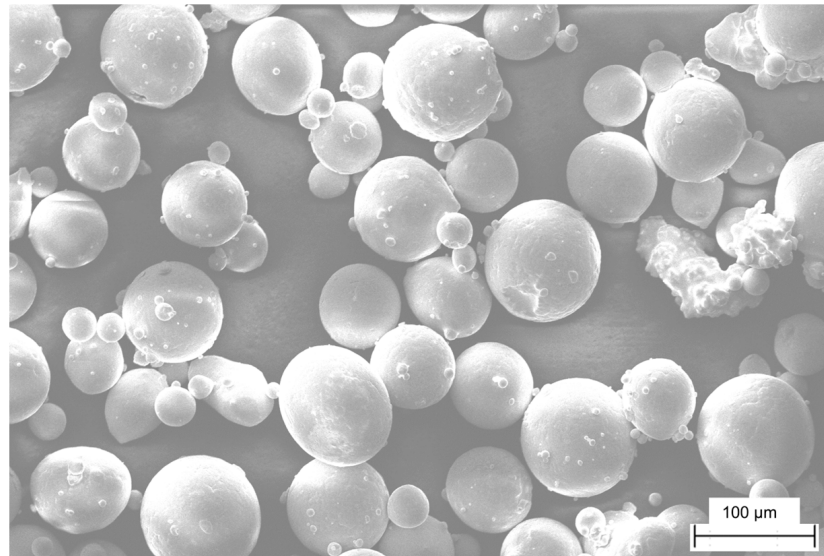

Figure 1. SEM image (image taken at 400× magnification) of the used Ti6Al4V powder for the DMD experiments.

The chemical composition of the powder and substrate used can be seen in Table 1.

Table 1. Chemical composition of the substrate and powder material in weight percentage.

	Ti	Fe	C	H	O	N	Al	V
Substrate	Bal.	0.17	0.013	0.002	0.115	0.0045	6.25	4.09
Powder	Bal.	0.24	0.002	0.002	0.05	0.004	6.34	4.25

Figure 2 shows the overall methodology used in this work. To investigate the influence of the gas flow settings (carrier gas flow and shield gas flow), they were varied on 6 different levels for two different nozzle geometries inside and without a shielding gas chamber. The remaining main machine parameters such as laser power, travel speed, and mass flow were kept constant. It should be mentioned that oxidation decreases with increasing mass flow (assuming constant travel speed and laser power), as part of the laser power is reflected and absorbed by the powder, so that a lower energy density is coupled into the substrate, which ultimately leads to lower temperatures and thus oxidation and vice versa. The travel speed was varied on three different levels. Detailed information can be found in the following explanations.

In order to evaluate the influence of the gas dynamics, the machine parameter laser power P = 1100 W, powder mass flow $\dot{m}$ = 4 g/min, and travel speed v = 720 mm/min were kept constant and only the carrier gas and shield gas volume flow were varied. Argon was used as the shielding gas and carrier gas volume flow species. The absolute volume fraction of argon is 99.998% and has the following impurities: H_2O < 3 ppm, O_2 < 2 ppm, N_2 < 10 ppm, CH_4 < 1 ppm, and CO_2 < 1 ppm. The variation of the gas flow settings can be seen in Table 2.
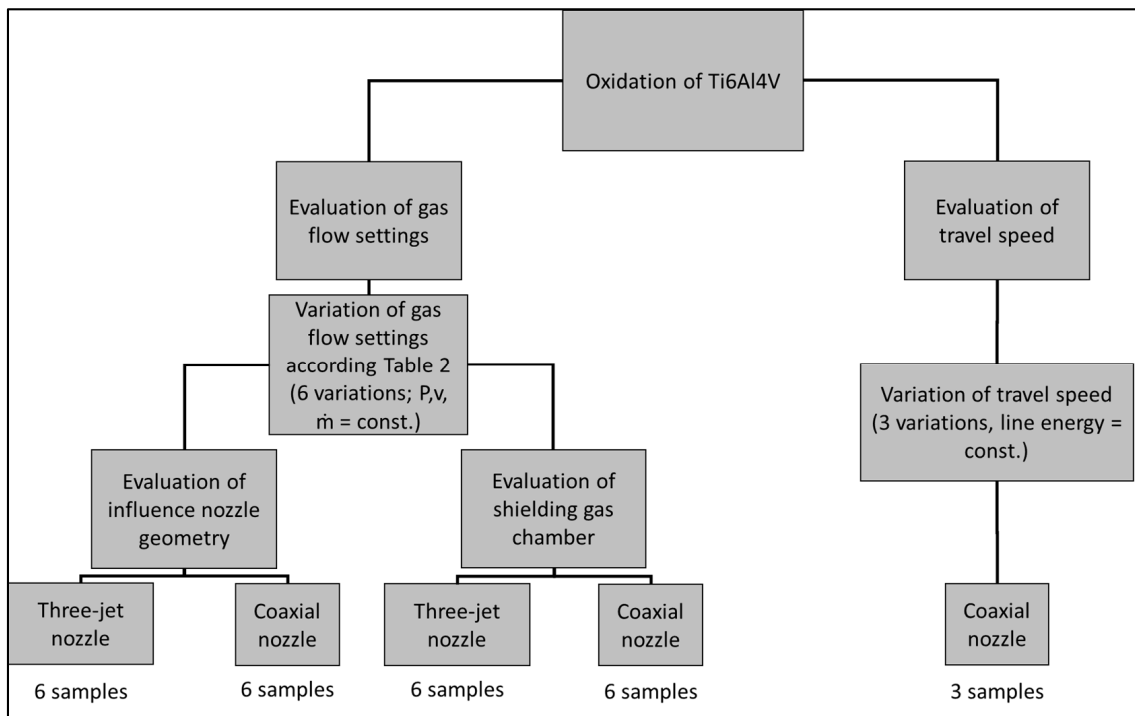
Figure 2. Methodology to determine the influence of gas flow settings, nozzle geometry, a shielding gas chamber, and travel speed on the oxidation of Ti6Al4V.

Table 2. Experimental plan for investigating the effects of gas flow settings, nozzle type, and shielding gas chamber on oxidation during the DMD process.

Experimental No.	Carrier Gas Flow (L/min)	Shield Gas Flow (L/min)	Carrier to Shield Gas Volume Flow Ratio	Nozzle Type	Shielding Gas Chamber
1	2	15	0.13		
2	2	30	0.07		
3	4	15	0.27	Three-jet/coaxial nozzle	Yes/No
4	4	30	0.13		
5	8	15	0.53		
6	8	30	0.27		

These experiments were carried out for both nozzle geometries, outside and inside a shielding gas chamber (as described in the work of Keller et al. [20]). To obtain a globally low oxygen concentration inside the chamber, the chamber was flooded with argon for 10 min before each experiment. It should be noted that there is a low residual oxygen concentration (<150 ppm) in the shielding gas chamber as upon initiation of powder flow, the activation of the machine suction system ensues, thereby facilitating the potential influx of external oxygen into the chamber interior. The permutation of the variables (nozzle geometry, buildup in shielding gas chamber/no shielding gas chamber) thus results in a total of 24 independent experiments (see left part in Figure 2). The additive structure had the following dimensions (see in Figure 3):
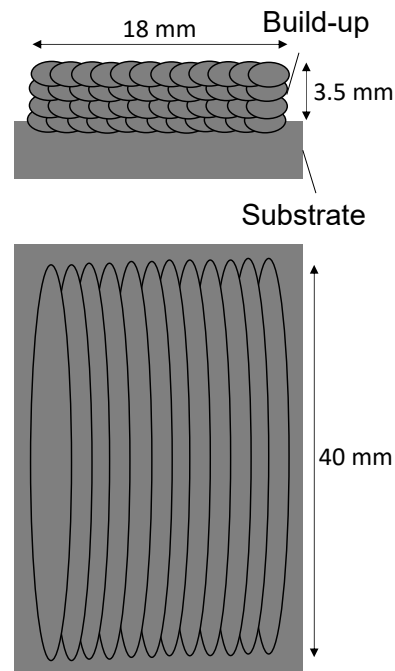
Figure 3. Schematic illustration of the additive buildups of the Ti6Al4V structures.

To finally assess the influence of the travel speed, the line energy E_l according to the formula,

$$E_l = \frac{P}{v} \qquad (3)$$

is kept constant, where P is the laser power and v is the travel speed. This ensures that the energy input is kept constant and thus a nearly equal build quality is achieved in terms of sufficient metallurgical bonding between the substrate and the build-up as well as a high-density buildup. In order to investigate the benefits of a heat sink with regard to oxidation, an experiment is carried out on a copper block. Figure 4 shows a schematic illustration of this experimental setup.
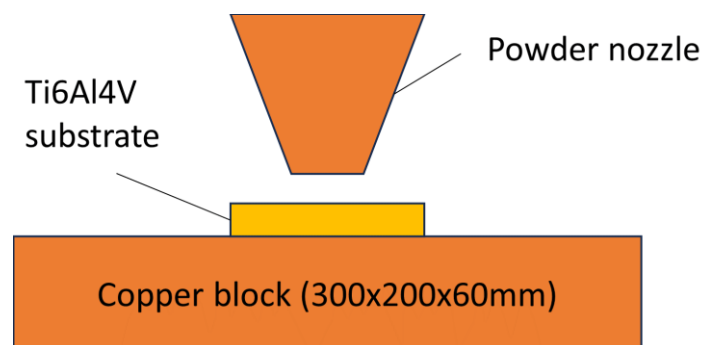
Figure 4. Schematic drawing of the experimental setup to investigate the usefulness of a copper block with regard to oxidation in the DMD process for Ti6Al4V.

To quantify the oxygen uptake, the hot carrier gas extraction (also inert gas fusion) method is used, which is approved according to standard ASTM E1409:13 [23] for the determination of the oxygen content in the titanium microstructure. The measuring instrument used was the LECO ONH836.

In order to ensure an accurate measurement of the hot carrier gas extraction method, cubes approximately equal to the weight of the calibration samples are required. For Ti6Al4V structures at a density of 100%, this corresponds to a cube with dimensions of $3 \times 3 \times 3$ mm. To achieve this height, 4 layers had to be built on top of each other. To ensure statistical

significance, 4 cubes were cut out of each buildup with wire EDM. To prevent falsification of the measurement results by the oxide layer on the sample cubes from the wire EDM cutting, the cube surfaces were ground until no oxide layer was visible on the cube surface under an optical microscope (Nikon C-PS (Nikon, Minato, Japan), magnification: 50×). For this, a SiC abrasive paper with 600 grit was used to prevent contamination from the normally used corundum grits. Afterwards, the cubes were cleaned with the device Bandelin Sonorex Digitec in pure ethanol in an ultrasonic bath for one minute in order to remove grinding residues. Then the cubes were air dried for at least 10 min. Figure 5 shows the procedure for determining the oxygen content in the Ti6Al4V microstructure.
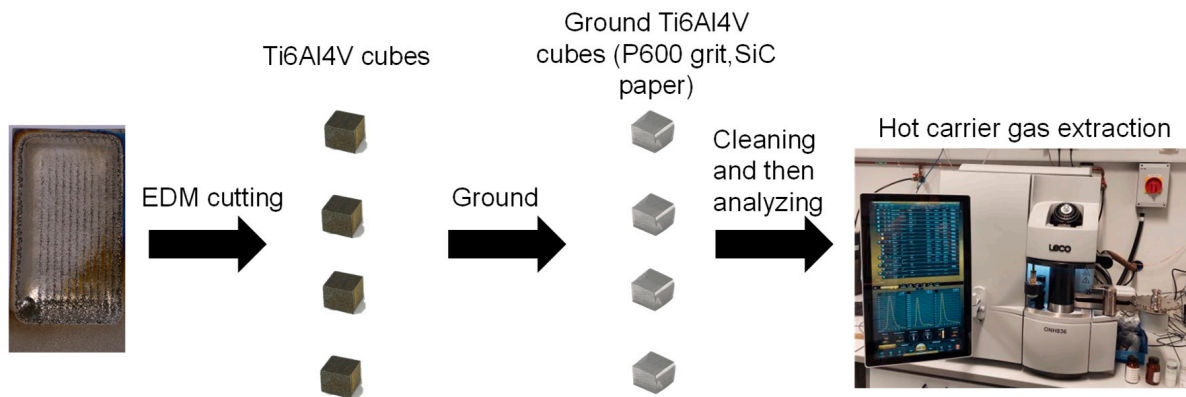

Figure 5. Flow diagram of the process for the determination of oxygen uptake by means of hot carrier gas extraction.

3. Results and Discussion

3.1. DMD Buildups without Shielding Gas Chamber

Figure 6 shows the oxygen concentration measured in the cubes extracted from the buildups produced with the three-jet nozzle for the different carrier gas (CG) to shield gas (SG) volume flow ratios without the shielding gas chamber.
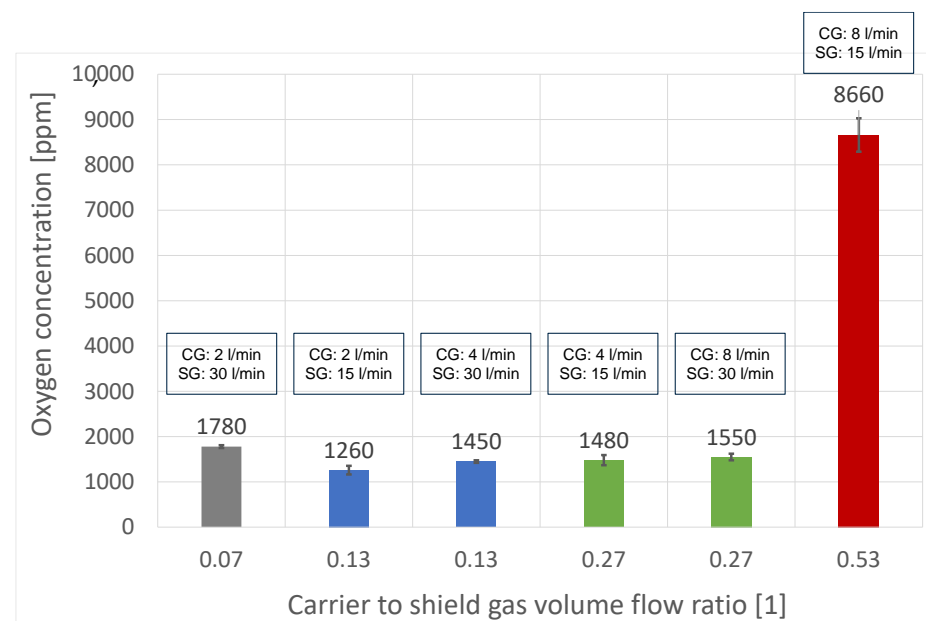

Figure 6. Oxygen uptake into the titanium microstructure produced using a three-jet nozzle for various carrier gas to shield gas flow ratios.

The bars in Figure 6 indicate the standard deviation of the measured oxygen concentration for all 4 cubes per gas flow setting. This also applies to all subsequent figures.

The oxygen concentration is lower than 2000 ppm for all samples built with a carrier to shield gas volume flow ratio less or equal to 0.27. However, the samples built with a higher ratio of 0.53 show a significantly higher oxygen intake, with more than 8500 ppm.

Figure 7 shows the oxygen concentration measured in the cubes extracted from the buildups produced with the coaxial nozzle for the different carrier gas to shield gas volume flow ratios without the shielding gas chamber.
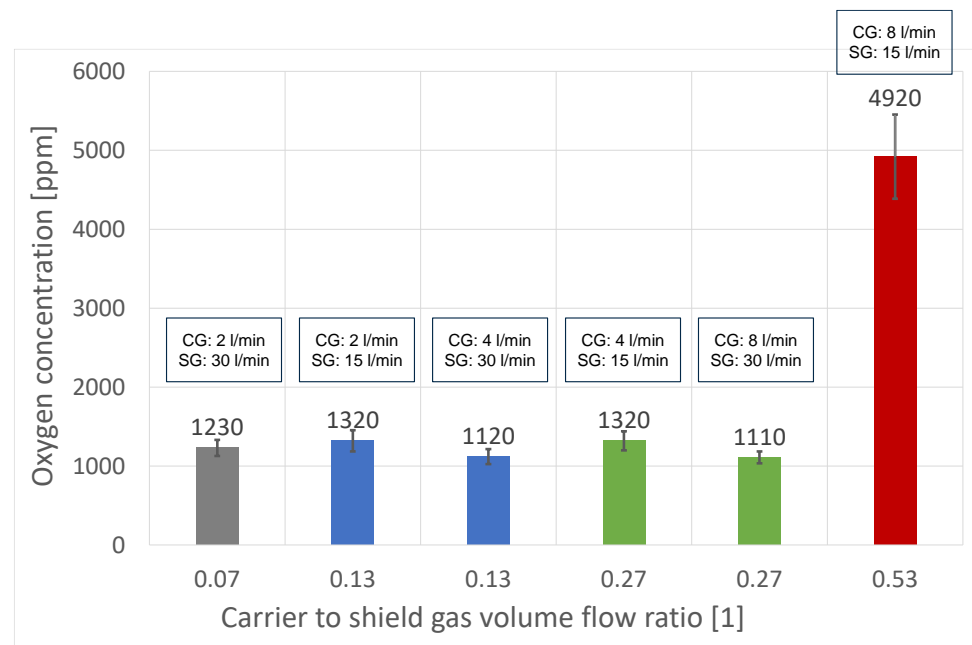

Figure 7. Oxygen uptake into the titanium microstructure produced using a coaxial nozzle for various carrier gas to shielding gas flows.

The oxygen concentration of the samples produced with the coaxial nozzle shows the same trend as the samples produced with the three-jet nozzle. The oxygen concentration is lower than 2000 ppm for all samples built with a carrier to shield gas volume flow ratio less or equal to 0.27. However, the samples built with a higher ratio of 0.53 show a significantly higher oxygen intake, with more than 4900 ppm.

The specifications for the aerospace industry require an oxygen concentration lower than 2000 ppm, and the medical industry requires below 1300 ppm. The results show that the standard for aerospace can be met with both nozzle geometries for a carrier to shield gas volume flow ratio inferior to 0.3. For higher ratios, the oxygen concentration increases drastically for both geometries. The specifications for the medical industry are not met by the samples built without the chamber.

The homogeneity of the oxygen uptake into the buildup decreases as the oxygen distribution of the shielding bell becomes inhomogeneous or is not given at all. Figure 8 shows a parameter sweep for various shielding gas and carrier gas volume flows.
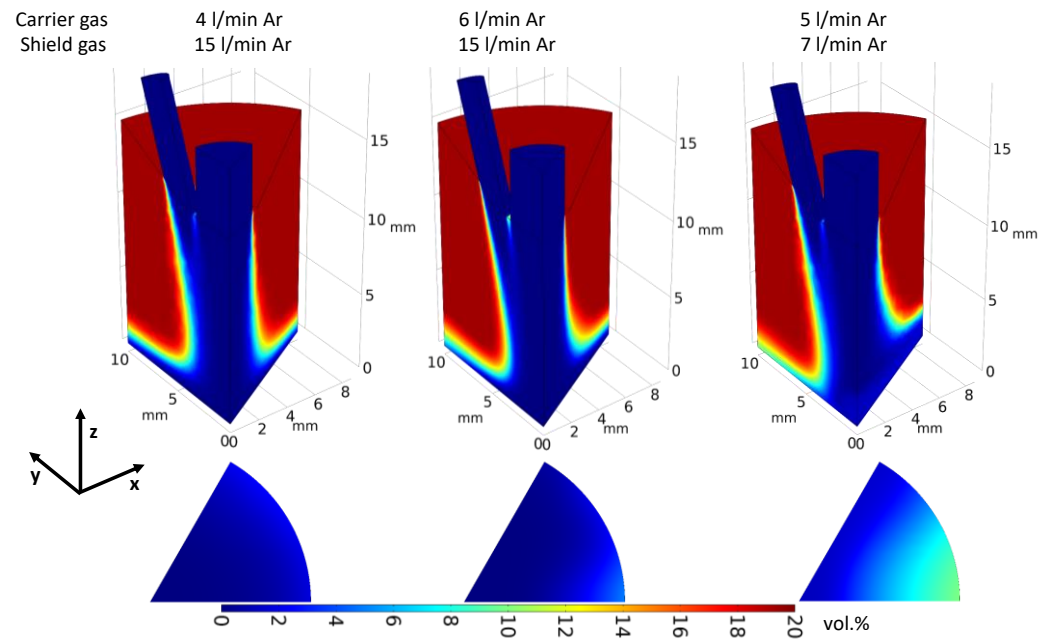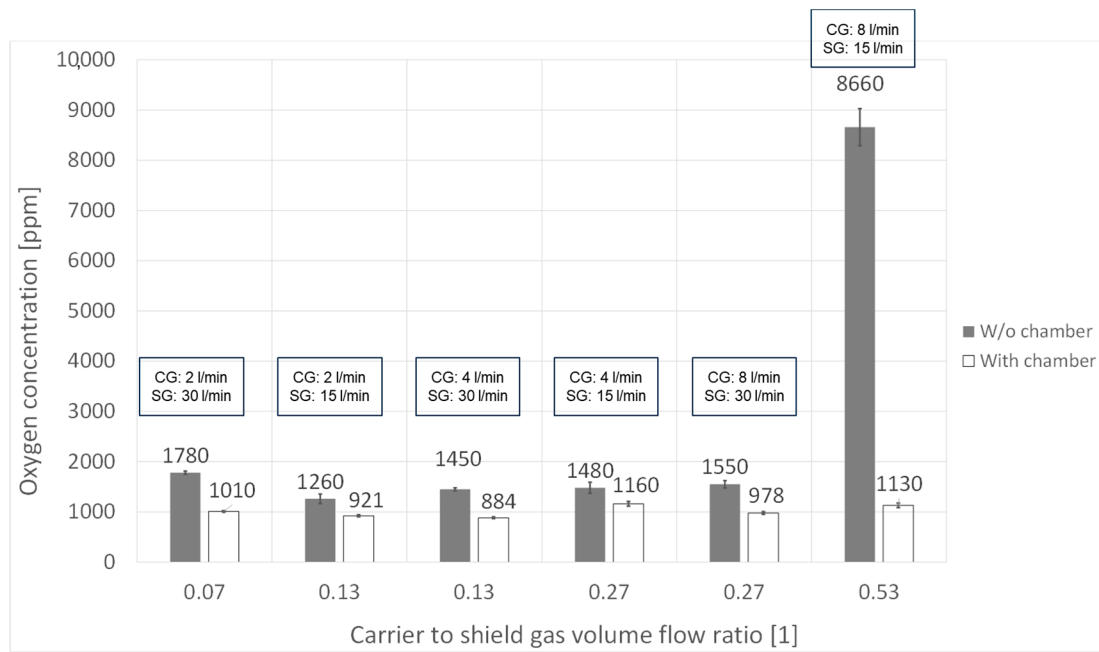
Figure 8. Simulation of the oxygen concentration of the three-jet nozzle for different carrier gas and shielding gas volume flows. The oxygen concentration increases drastically as the carrier gas to shielding gas volume flow ratio increases. The figure is based on [20].

Figure 8 shows that the oxygen concentration in the powder focus (circle section at the bottom of Figure 8) increases with an increasing carrier gas to shielding gas volume flow ratio. For the simulation on the right in Figure 8, sufficient shielding gas shielding is only provided exactly in the center. The shielding decreases drastically towards the outside. This is primarily due to the following two effects:
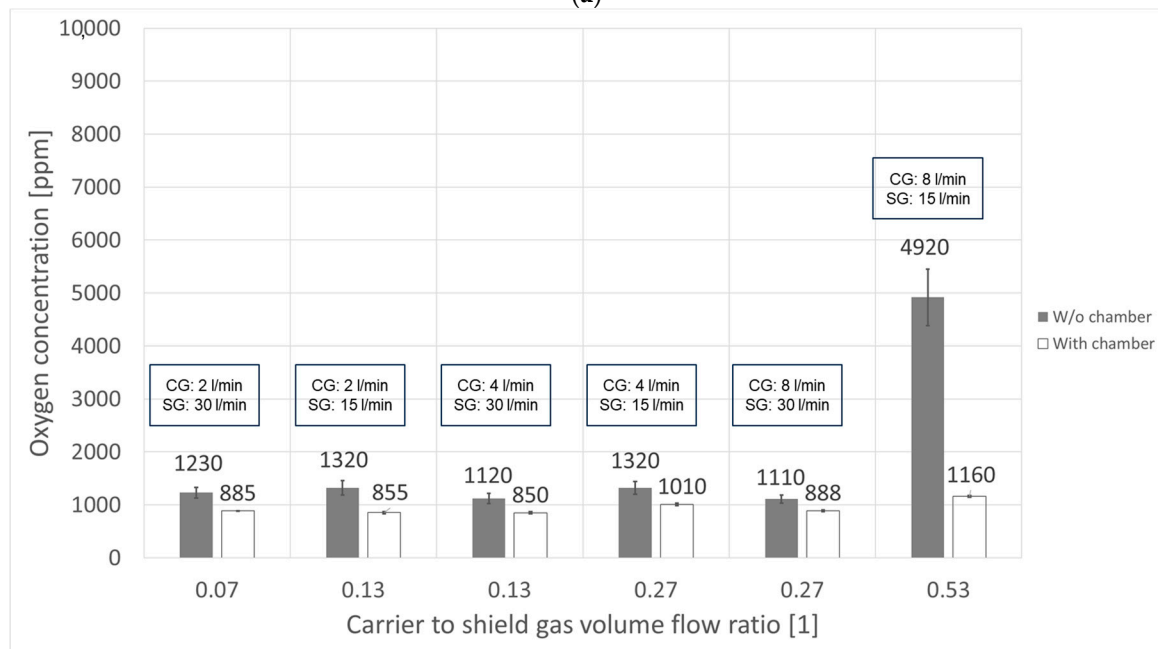
- Due to the relatively stronger carrier gas flow with increasing carrier gas to shielding gas flow ratio, the impulse that the carrier gas flow exerts on the shielding gas flow increases. This leads to a higher degree of momentum transfer. The increase in momentum, however, can result in the induction of turbulence within the gas flow. This turbulence manifests as chaotic and irregular movements of the gases within the welding environment. Turbulence in the gas flow dynamics can have deleterious effects, particularly in the welding context. One significant consequence is the introduction of oxygen into the shielding gas zone. The degree of oxidation because of these gas flow dynamics is quantified in this work.
- Due to the higher carrier gas flow, the flow velocity of the carrier gas increases. The higher velocity causes the static pressure within the gas to decrease, as Bernoulli states that the total pressure is constant and results from the sum of the static pressure and the dynamic pressure. As the flow velocity increases, the dynamic pressure increases (proportional to the square of the velocity) and consequently the static pressure within the gas decreases. This negative pressure sucks ambient gas into the carrier gas flow, allowing oxygen to enter the shielding gas zone and increase the oxidation.

3.2. DMD Buildups with Shielding Gas Chamber

The oxygen concentrations in the DMD buildups produced inside the shielding gas chamber are shown for the three-jet nozzle in Figure 9a and for the coaxial nozzle in Figure 9b.

Figure 9. Influence of the shielding gas chamber on oxygen uptake into the titanium microstructure for (**a**) three-jet nozzle and (**b**) coaxial nozzle for various carrier gas to shield gas volume flow ratios.

Figure 9 shows a significant reduction in oxygen uptake into the titanium structure when the shielding gas chamber is used compared to the same process conditions without a chamber. For all carrier to shield gas volume flow ratios, both aerospace and medical standards are met, with all samples displaying an oxygen concentration below 1300 ppm. The standard deviations observed are also minimized, showing a better homogeneity of the oxygen intake in the buildups with the use of the chamber. However, a subtle oxidation persists due to the residual oxygen content within the chamber being less than 150 ppm, as elucidated in the experimental section.

A shielding gas chamber allows for medical-standard parts to be produced by DMD regardless of the optimization of the carrier to shield gas volume flow ratio.

3.3. DMD Buildups without Shielding Gas Chamber at Varied Travel Speed

In addition to the influence of the gas dynamics, which are determined by the carrier gas to shield gas volume flow ratio, the influence of the travel speed was also investigated by varying the travel speed. The objective of this investigation is to assess the feasibility of constructing Ti6Al4V components that meet oxidation criteria through the DMD process with an adequate level of reliability, even in the absence of a shielding gas chamber. To make the process as comparable as possible to the temperature distribution, the line energy was kept constant at approximately 92 J/mm with $P = 1100$ W and $v = 720$ mm/min = 12 mm/s. Figure 10 shows the oxygen concentration in the DMD buildups produced with the coaxial nozzle for different travel speeds.
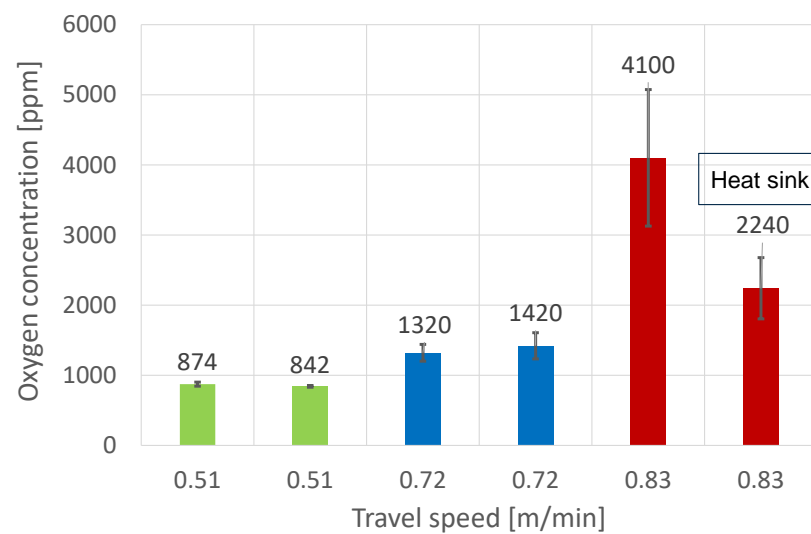

Figure 10. Oxygen uptake into the titanium microstructure using a coaxial nozzle for various travel speeds at constant line energy and constant carrier to shield gas volume flow ratio (CG: 4 L/min, SG: 15 L/min). The rightmost bar shows the benefit of using a heat sink at increased feed rates to reduce oxidation.

Figure 10 shows that reducing the travel speed to 0.51 m/min (at constant line energy) fulfills the oxygen limits for the aerospace and medical industries, such that they are met even without the use of a shielding gas chamber. At lower travel speeds, the melt pool and the hot, already solidified material remain longer in the area of the shielding gas bell. For DMD typical cooling rates approaching up to 1000 K/s [24,25], the material can thus cool down sufficiently so that the material oxidizes less.

Increasing the travel speed, on the other hand, leads to a sharp increase in oxygen uptake into the titanium structure. Oxidation can be significantly reduced with a heat sink. The thermal resistance of a series connection of two different materials can be described according to Holman [26] by the following equation:

$$R_{sc} = R_{th,1} + R_{th,2} = \frac{l_{Cu}}{k_{Cu}A} + \frac{l_{Ti6Al4V}}{k_{Ti6Al4V}A} = \frac{l_{Cu} + l_{Ti6Al4V}}{k_{sc}A},$$

where k_{Cu} is the thermal conductivity of copper, $k_{Ti6Al4V}$ is the thermal conductivity of Ti6Al4V, l_{Cu} is the thickness of the copper block, and $l_{Ti6Al4V}$ is the thickness of the titanium substrate perpendicular to the heat flux over the cross-sectional area A. This results in a thermal conductivity of the series connection of the two materials according to:

$$k_{sc} = \frac{k_{Cu}k_{Ti6Al4V}(l_{Cu} + l_{Ti6Al4V})}{k_{Cu}l_{Ti6Al4V} + k_{Ti6Al4V}l_{Cu}}$$

With a thermal conductivity of Ti6Al4V $k_{Ti6Al4V} = 17.5$ W/mK (at 800 °C, [27]), thickness $l_{Ti6Al4V} = 6$ mm, thermal conductivity of copper $k_{Cu} = 366$ W/mK (at 800 °C, [28]), and thickness $l_{Cu} = 50$ mm of the Ti6Al4V substrate, the resulting thermal conductivity is $k_{sc} = 116.8$ W/mK. This is greater than that of Ti6Al4V by a factor of 6.7. Thus, due to the high thermal conductivity, the heat from the titanium substrate and the deposited Ti6Al4V can be dissipated more quickly, thus the oxidation rate is reduced due to the lower temperature of the material outside the shielding gas bell.

This study investigated the impact of gas flow settings and travel speed on the oxidation of Ti6Al4V. The results demonstrate that a carrier gas to shield gas volume flow ratio of <0.3 is necessary to produce components with suitable oxygen concentrations in the Ti6Al4V microstructure, employing both three-jet and coaxial nozzle configurations. Additionally, it was observed that the parameter of line energy, as commonly cited in the literature, is insufficient for describing the temperature field adequately.

Under constant line energy conditions, tests conducted at higher travel speeds exhibited a significantly higher level of oxidation, while lower travel speeds resulted in reduced oxidation. This occurred despite maintaining a carrier gas to shield volume flow ratio <0.3. The study underscores that the requirements of medical technology, specifically the oxygen limit below 1300 ppm, can be met at lower travel speeds.

The current quasi-static analysis, as performed in the work of Keller et al. [20], has limitations. The ratio of 0.3 is a necessary condition for achieving a sufficiently low oxygen concentration, but it must be overlaid with the travel speed. Higher travel speeds lead to reduced heat dissipation, causing the temperature field with oxidation-critical temperatures to extend over a larger range, resulting in higher oxidation. The benefit of using a heat sink to reduce oxidation at higher travel speeds was demonstrated.

The paper suggests developing an oxidation model that overlays the temperature field with spatial oxygen concentration to predict oxidation more accurately. The issue with one of the latest oxidation models of Ti alloys from the work of Vaché et al. [29] lies in considering purely parabolic oxidation kinetics, which are no longer valid at elevated temperatures (above 600 °C). In the DMD process, a prerequisite is that the material being deposited is melted (temperatures greater than 1650 °C are necessary). Furthermore, the aforementioned oxidation model describes oxidation under isothermal conditions and durations of several hours. However, the DMD process involves complex thermal temperature fields and temperature gradients with oxidation-critical temperatures lasting only a few seconds. As a result, the most recent oxidation model is not applicable to the DMD process. Additionally, other methods for preventing oxidation through nitrogen, as described in the work of Dupressoire et al. [30] using interfacial layers of oxynitrides and nitrides, are not feasible in the DMD process since the gas flow species in the carrier and shielding gas streams is argon. This necessitates conducting a temperature field simulation. This could ultimately form the basis for defining a parameter that predicts whether the DMD process is oxidation-critical or not, accounting for the dynamics of the process appropriately. Furthermore, mechanical properties (such as hardness, microstructure, tensile strength, and other mechanical characteristics) must be specified, which are caused by the varying degrees of oxidation. Another future research idea is to improve the shielding during the DMD process, as handling the shielding gas chamber is cumbersome. To this end, concepts need to be considered that do align with the findings of an oxidation model.

4. Conclusions

Ti6Al4V samples complying with aerospace and medical standards concerning oxygen intake have been produced by DMD. The geometry of the nozzle (coaxial or three-jet) is secondary compared to the optimization of the shielding conditions. For both nozzle geometries, the optimization of the carrier to shield gas volume flow ratio permits achieving aerospace quality parts (<2000 ppm) without a shielding gas chamber, and medical quality (<1300 ppm) when a shielding gas chamber is used. Yet, both quality standards can be met without a shielding gas chamber by adjusting the travel speed.

- For a carrier gas to shield a gas volume flow ratio <0.3, the aerospace industry limitations regarding oxygen uptake (<2000 ppm) can be met for both nozzle types without a shielding chamber.
- By reducing the travel speed, the limits for the medical industry can be achieved even without the usage of a shielding gas chamber.
- An increased travel speed leads to the maximum permitted oxygen concentration of 2000 ppm being exceeded for the same specific energy. Oxidation can be reduced by using a copper block that functions as a heat sink.
- With higher carrier to shield gas volume flow ratios, the homogeneity of the oxygen uptake in the part decreases and vice versa. This phenomenon is explicable through the interplay of turbulent flow characteristics within the shielding gas bell jar and the Bernoulli effect. Elevated velocities of the carrier gas flow induce a negative pressure, which causes an ingress of oxygen from the ambient surroundings, facilitating its transport to the surface of the Ti6Al4V material.

References

1. Dass, A.; Moridi, A. State of the Art in Directed Energy Deposition: From Additive Manufacturing to Materials Design. *Coatings* **2019**, *9*, 418. [CrossRef]
2. Hosseini, E.; Popovich, V.A. A review of mechanical properties of additively manufactured Inconel 718. *Addit. Manuf.* **2019**, *30*, 100877. [CrossRef]
3. LiLiu, G.; Zhang, X.; Chen, X.; He, Y.; Cheng, L.; Huo, M.; Yin, J.; Hao, F.; Chen, S.; Wang, P.; et al. Additive manufacturing of structural materials. *Mater. Sci. Eng. R Rep.* **2021**, *145*, 100596. [CrossRef]
4. Moradi, M.; Pourmand, Z.; Hasani, A.; Moghadam, M.K.; Sakhaei, A.H.; Shafiee, M.; Lawrence, J. Direct laser metal deposition (DLMD) additive manufacturing (AM) of Inconel 718 superalloy: Elemental, microstructural and physical properties evaluation. *Optik* **2022**, *259*, 169018. [CrossRef]
5. Nankali, M.; Akbari, J.; Moradi, M.; Beiranvand, Z.M. Effect of laser additive manufacturing parameters on hardness and geometry of Inconel 625 parts manufactured by direct laser metal deposition. *Optik* **2022**, *249*, 168193. [CrossRef]
6. Kumar, S.P.; Elangovan, S.; Mohanraj, R.; Ramakrishna, J.R. A review on properties of Inconel 625 and Inconel 718 fabricated using direct energy deposition. *Mater. Today Proc.* **2021**, *46*, 7892–7906. [CrossRef]
7. Mukherjee, T.; Manvatkar, V.; De, A.; DebRoy, T. Dimensionless numbers in additive manufacturing. *J. Appl. Phys.* **2017**, *121*, 064904. [CrossRef]
8. Ashkani, O.; Tavighi, M.R.; Karamimoghadam, M.; Moradi, M.; Bodaghi, M.; Rezayat, M. Influence of Aluminum and Copper on Mechanical Properties of Biocompatible Ti-Mo Alloys: A Simulation-Based Investigation. *Micromachines* **2023**, *14*, 1081. [CrossRef]
9. Niinomi, M. Biologically and mechanically biocompatible titanium alloys. *Mater. Trans.* **2008**, *49*, 2170–2178. [CrossRef]
10. Gepreel, M.A.H.; Niinomi, M. Biocompatibility of Ti-alloys for long-term implantation. *J. Mech. Behav. Biomed. Mater.* **2013**, *20*, 407–415. [CrossRef]
11. Baltatu, M.S.; Tugui, C.A.; Perju, M.C.; Benchea, M.; Spataru, M.C.; Sandu, A.V.; Vizureanu, P. Biocompatible titanium alloys used in medical applications. *Rev. Chim.* **2019**, *70*, 1302–1306. [CrossRef]
12. Amherd Hidalgo, A.; Frykholm, R.; Ebel, T.; Pyczak, F. Powder metallurgy strategies to improve properties and processing of titanium alloys: A review. *Adv. Eng. Mater.* **2017**, *19*, 1600743. [CrossRef]
13. Qian, M. (Ed.) *Powder Metallurgy of Titanium*; Trans Tech Publications Ltd.: Bäch, Switzerland, 2012.
14. Gurrappa, I. An oxidation model for predicting the life of titanium alloy components in gas turbine engines. *J. Alloys Compd.* **2005**, *389*, 190–197. [CrossRef]

15. Casadebaigt, A.; Hugues, J.; Monceau, D. High temperature oxidation and embrittlement at 500–600 °C of Ti-6Al-4V alloy fabricated by Laser and Electron Beam Melting. *Corros. Sci.* **2020**, *175*, 108875. [CrossRef]

16. Guleryuz, H.; Cimenoglu, H. Oxidation of Ti–6Al–4V alloy. *J. Alloys Compd.* **2009**, *472*, 241–246. [CrossRef]

17. Du, H.L.; Datta, P.K.; Lewis, D.B.; Burnell-Gray, J.S. Air oxidation behaviour of Ti 6Al 4V alloy between 650 and 850°. *Corros. Sci.* **1994**, *36*, 631–642. [CrossRef]

18. Yu, C.; Zhu, S.; Wei, D.; Wang, F. Oxidation and H2O/NaCl-induced corrosion behavior of sputtered Ni–Si coatings on Ti6Al4V at 600–650° C. *Surf. Coat. Technol.* **2007**, *201*, 7530–7537. [CrossRef]

19. Coddet, C.; Craze, A.M.; Beranger, G. Measurements of the adhesion of thermal oxide films: Application to the oxidation of titanium. *J. Mater. Sci.* **1987**, *22*, 2969–2974. [CrossRef]

20. Keller, D.; Monney, A.; Schudeleit, T.; Wegener, K. Spatial Oxygen Distribution of the Direct Metal Deposition Process for Different Powder Nozzles. *Appl. Sci.* **2023**, *13*, 9470. [CrossRef]

21. *DIN 17850*; Titanium—Chemical Composition. Available online: https://www.beuth.de/de/norm/din-17850/370729589 (accessed on 27 December 2023).

22. *DIN 17851*; Titanium Alloys—Chemical Composition. Available online: https://www.beuth.de/de/norm/din-17851/370729621 (accessed on 27 December 2023).

23. *ASTM E1409:13*; Standard Test Method for Determination of Oxygen and Nitrogen in Titanium and Titanium Alloys by Inert Gas Fusion. Available online: https://www.astm.org/e1409-13r21.html (accessed on 27 December 2021).

24. Li, J.; Yu, Z.; Wang, H.; Li, M. Microstructural characterization of titanium matrix composite coatings reinforced by in situ synthesized TiB+ TiC fabricated on Ti6Al4V by laser cladding. *Rare Met.* **2010**, *29*, 465–472. [CrossRef]

25. Yuan, W.; Li, R.; Chen, Z.; Gu, J.; Tian, Y. A comparative study on microstructure and properties of traditional laser cladding and high-speed laser cladding of Ni45 alloy coatings. *Surf. Coat. Technol.* **2021**, *405*, 126582. [CrossRef]

26. Holman, J.P. *Heat Transfer*; McGraw Hill: New York, NY, USA, 1986.

27. Childs, T.H. *Metal Machining: Theory and Applications*; Butterworth-Heinemann: Oxford, UK, 2000.

28. Ho, C.Y.; Powell, R.W.; Liley, P.E. Thermal conductivity of the elements. *J. Phys. Chem. Ref. Data* **1972**, *1*, 279–421. [CrossRef]

29. Vaché, N.; Cadoret, Y.; Dod, B.; Monceau, D. Modeling the oxidation kinetics of titanium alloys: Review, method and application to Ti-64 and Ti-6242s alloys. *Corros. Sci.* **2021**, *178*, 109041. [CrossRef]

30. Dupressoire, C.; Descoins, M.; Put, A.V.; Epifano, E.; Mangelinck, D.; Emile, P.; Monceau, D. The role of nitrogen in the oxidation behaviour of a Ti6242S alloy: A nanoscale investigation by atom probe tomography. *Acta Mater.* **2021**, *216*, 117134. [CrossRef]